A Potential-based Formulation for Motion-Induced Electric Fields in MRI

Published paper @DOI: 10.1109/TMAG.2015.2474748



# A Potential-based Formulation for Motion-Induced Electric Fields in MRI

L. Zilberti[1], O. Bottauscio[1], *Senior Member IEEE*, and M. Chiampi[2]

[1]Istituto Nazionale di Ricerca Metrologica, Torino, 10135, Italy
[2]Dipartimento Energia, Politecnico di Torino, Torino, 10135, Italy

**This paper presents a potential-based formulation conceived to estimate the electric field induced in a human body moving through the stray stationary magnetic field produced by magnetic resonance scanners. Two different descriptions are adopted, giving rise to two different driving terms, and the corresponding electromagnetic problems are solved numerically, according to a Finite Element approach. The application of the procedure recommended by the ICNIRP Guidelines to perform the exposure assessment is discussed and some examples, which refer to a realistic situation, are finally presented.**

***Index Terms*— Magnetic resonance imaging, Motion induced electric field, Human exposure, Finite element method.**

## I. Introduction

ATTENTION has been often paid to dosimetric aspects in Magnetic Resonance Imaging (MRI) environments, making reference mainly to the effects produced by gradient and radiofrequency coils on the human body (e.g. see [1], [2]). More recently, an increasing interest has been devoted to the exposure of the medical staff moving through the strong (on the order of 1 T) stray stationary magnetic field of MRI scanners. This kind of exposure may provoke transient annoying symptoms (vertigo, nausea, magnetophosphenes and peripheral nerve stimulation), which are not considered directly detrimental, but can impair working ability. These circumstances reflect indirectly on patients' safety and, therefore, also on the development of innovative applications (e.g. MRI-guided surgery). In order to regulate the situation, in March 2014 the International Commission on Non-Ionizing Radiation Protection (ICNIRP) published specific Guidelines providing exposure limits [3]. In particular, basic restrictions to prevent from magnetophosphenes and peripheral nerve stimulation have been set in terms of induced electric field. As already happened for the exposure to sinusoidal fields, in the future the Guidelines probably will be included in some legislative measure (e.g. the European Directive addressing workers' exposure to electromagnetic fields). This calls for dedicated computational techniques able to estimate such an electric field. Even though some numerical analyses of motion-induced fields in MRI have been already presented (e.g. [4]-[8]), none of them was based on the Guidelines now in force. Thus, starting from two computational schemes (one recently proposed by the authors [4] and the other presented in [6]) this paper deepens some aspects of the problem and discusses the application of the new ICNIRP Guidelines to perform the exposure assessment under realistic conditions.

Manuscript received June 23, 2015; revised XXX, 2015; accepted XXX, 2015. Date of publication XXX, 2015; date of current version XXX, 2015. Corresponding author: L. Zilberti (e-mail: l.zilberti@inrim.it).

Color versions of one or more of the figures in this paper are available online at http://ieeexplore.ieee.org.

Digital Object Identifier (inserted by IEEE).

## II. Method

### A. Formulation

The electromagnetic induction due to the motion of the body through a magnetic field is described from two different viewpoints: reference frame R, at rest with respect to the field sources, and reference M, co-moving with the body. Physical quantities referred to a specific reference are identified by the corresponding subscript. The velocity of a point belonging to the moving body, measured in R, is $\boldsymbol{v}(x,y,z,t)$.

Given the features of the problem, the formulation is developed according to the "Galilean Magnetic Limit approximation" [9], which leads to the following transformations for the magnetic flux density, the corresponding vector potential and the electric field:

$$\boldsymbol{B}_{\mathrm{M}} = \boldsymbol{B}_{\mathrm{R}} = \boldsymbol{B} \tag{1a}$$

$$\boldsymbol{A}_{\mathrm{M}} = \boldsymbol{A}_{\mathrm{R}} = \boldsymbol{A} \tag{1b}$$

$$\boldsymbol{E}_{\mathrm{M}} = \boldsymbol{E}_{\mathrm{R}} + \boldsymbol{v} \times \boldsymbol{B} \tag{1c}$$

(note that the invariance of $\boldsymbol{B}$ and $\boldsymbol{A}$ among the reference frames does not imply the same invariance for their time-derivatives). The values of both $\boldsymbol{v}$ and its rate of change (i.e. the acceleration) are relatively low (consistent with human movements) and allow assuming the relevant Maxwell's equations as covariant between R and M, even when the latter is non-inertial [10], [11]. The currents induced within the human body are considered too low to perturb the distribution of $\boldsymbol{B}$ (i.e. $\boldsymbol{B}$ is impressed by the external sources) and, as already discussed [4], in general their dielectric component can be disregarded when computing motion-induced electric fields. Moreover, in the air region outside the body the dielectric currents are neglected as well, obtaining that the normal component of the induced current density must be null along the external boundary. In R the electric field is curl-free (because $\boldsymbol{B}$ has no time-derivative) and can be represented simply through a scalar potential. In M, the flux density

appears to be time-varying and therefore the electric field is represented by both a scalar and a vector potential:

$$\boldsymbol{E}_{\mathrm{R}} = -\nabla\varphi_{\mathrm{R}} \tag{2a}$$

$$\boldsymbol{E}_{\mathrm{M}} = -\left[\frac{\partial \boldsymbol{A}}{\partial t}\right]_{\mathrm{M}} - \nabla\varphi_{\mathrm{M}} \tag{2b}$$

Equation (2b) expresses the electric field experienced by the moving body (i.e. the quantity to be monitored) directly in terms of quantities defined in M. Taking into account (1c) and (2a), the same electric field can be also represented through the quantities measured by an observer at rest in R:

$$\boldsymbol{E}_{\mathrm{M}} = -\nabla\varphi_{\mathrm{R}} + \boldsymbol{v}\times\boldsymbol{B} \tag{3}$$

Note that, in general, $\boldsymbol{v}\times\boldsymbol{B} \neq -\left[\partial\boldsymbol{A}/\partial t\right]_{\mathrm{M}}$ and therefore also $\varphi_{\mathrm{R}} \neq \varphi_{\mathrm{M}}$, even if, of course, (2b) and (3) must be equivalent (see the Appendix for a formal proof).

If $\sigma$ is the electrical conductivity, $\sigma\boldsymbol{E}_{\mathrm{M}}$ is the current density in frame M. Disregarding dielectric effects, such current density is divergence-free. Thus, from (2b) and (3) we get:

$$\nabla\cdot\left[\sigma\left(\nabla\varphi_{\mathrm{M}}\right)\right] = -\nabla\cdot\left[\sigma\left(\frac{\partial \boldsymbol{A}}{\partial t}\right)_{\mathrm{M}}\right] \tag{4a}$$

$$\nabla\cdot\left[\sigma\left(\nabla\varphi_{\mathrm{R}}\right)\right] = \nabla\cdot\left[\sigma\left(\boldsymbol{v}\times\boldsymbol{B}\right)\right] \tag{4b}$$

Passing to the classical "weak form", suitable for a Finite Element (FE) numerical implementation, and taking into account the boundary conditions mentioned above, these equations give rise respectively to the two problems [4], [6]:

$$\int_{\Omega}\left\{\left[\sigma\left(\nabla\varphi_{\mathrm{M}}\right)\right]\cdot\nabla w\right\}dv = -\int_{\Omega}\left\{\left[\sigma\left(\frac{\partial \boldsymbol{A}}{\partial t}\right)_{\mathrm{M}}\right]\cdot\nabla w\right\}dv \tag{5a}$$

$$\int_{\Omega}\left\{\left[\sigma\left(\nabla\varphi_{\mathrm{R}}\right)\right]\cdot\nabla w\right\}dv = \int_{\Omega}\left\{\left[\sigma\left(\boldsymbol{v}\times\boldsymbol{B}\right)\right]\cdot\nabla w\right\}dv \tag{5b}$$

where $\Omega$ is the computational domain (i.e. the body) and $w$ is the test function. Both versions have been implemented into homemade computational codes based on the FE approximation, using nodal unknowns. In view of their direct application to high-resolution voxel-based human models, hexahedral elements with trilinear shape functions have been chosen. Since the magnetic field is considered impressed by the external sources, the right-hand sides of (5a) and (5b) act as driving terms. In order to improve the computational efficiency, the distributions of the flux density and of a Coulomb-gauged vector potential are computed preliminarily, once and for all. This is done on a regular grid of points around the sources (the region where the motions will take place), through a classical Biot-Savart integration applied to the sources themselves (current-carrying coils). Starting from the initial position of the body, a motion trajectory (which can include any rigid translation and/or rotation, performed with a time-dependent velocity) is defined in R and discretized into time steps. Hence, the positions taken up by the barycenters of all elements along the trajectory is determined (in R). For each step, the values of $\boldsymbol{B}$ and $\boldsymbol{A}$ in all barycenters are computed by interpolation within the grid. When solving (5a) at a given step $s$, the components of the vector potential evaluated for each barycenter are projected on the co-moving frame M and then used to compute the time-derivative required by (5a) through an incremental ratio across steps ($s$+1) and ($s$–1). In problem (5b), at a given step $s$ the velocity associated to each barycenter is computed as an incremental ratio between its positions (indicated by the vectorial distance from the origin of R) at the following ($s$+1) and previous ($s$–1) instants. Then, the vector product which acts as a driving term in (5b) is determined for all elements and instants, and finally projected on the axes of M (this latter operation allows obtaining the values of $\boldsymbol{E}_{\mathrm{M}}$ directly in the reference frame of the body). In order to remove the degree of freedom implied by the use of a scalar potential, during the solution of both (5a) and (5b) its value is fixed to zero in one node of the mesh.

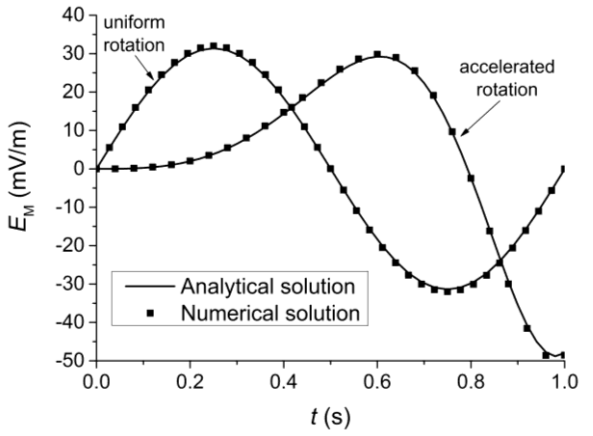


Fig. 1. Validation of the numerical codes (parameter $x_0$ set to 0.01 m).

Taking advantage of the band-structured stiffness matrix, determined by the regular voxel-based mesh, a Cholesky-like decomposition is exploited in GPU environment (using NVIDIA CUDA library) to speed-up the solver phase. The electric field experienced by the moving body is finally reconstructed according to either definition (2b) or (3).

### *B. Validation*

An experimental validation of predicted motion-induced fields is almost unfeasible in vivo. Moreover, it must be noted that the use of an induction probe would be of low usefulness in this context, because such probes actually measure the rate of change of a magnetic flux. This information is associated to the circulation of an electric field (whose value depends on the size of the probe), but does not provide directly the local value of the field itself (which, in general, depends on interfaces and boundaries). For these reasons, a validation of the computational tools through comparison with analytical solutions appears as the most suitable choice. The comparison presented here considers a homogeneous non-magnetic disk, with negligible thickness, rotating through a stationary, uniform and unitary distribution of magnetic flux density directed along $z$. At the starting position the two frames R and M coincide, the disk lies on the $xy$-plane and its centre is placed at the origin of the axes. In a first test, the disk rotates around the $x$-axis, with a uniform angular speed of $2\pi$ rad/s. The numerical solution is compared with the analytical one, considering the same disk at rest, but immersed in a uniform, $z$-directed, time-varying magnetic flux density $B_1 = \cos(2\pi t)$. In the second test, the disk rotates again about the $x$-axis, but

TABLE I
BASIC RESTRICTIONS

| Frequency range (Hz) | $L$ (V/m) | $\delta$ (°) |
|---|---|---|
| 0 – 0.66 | 1.1 | 0 |
| 0.66 – 10 | $0.7/f$ | 90 |
| 10 – 25 | 0.07 | 0 |
| 25 – 400 | $2.83 \cdot 10^{-3} \cdot f$ | -90 |

with an angular speed that increases linearly (angular acceleration $\alpha$ = 10 rad/s$^2$). The numerical solution is compared with the analytical relation describing the electric field induced in the same disk at rest, immersed in a uniform, $z$-directed, time-varying magnetic flux density $B_2 = \cos(\alpha t^2/2)$. The results are presented in Fig. 1, with reference to the $y$-component of $E_M$ in point $(x_0, 0, 0)_M$. The other two components, null in the analytical solution, are some orders of magnitude smaller in the numerical solutions. The results obtained by solving (5a) and (5b) are practically indistinguishable among each other (discrepancy lower than 0.1 %) and therefore presented as a single result. For both tests the agreement with the reference solution is excellent.

### C. Possible extension to dielectric effects

As discussed in [4], despite the very high permittivity ($\varepsilon$) attributed to biological tissues at low frequency, at a first approximation the dielectric effects can be disregarded when computing motion-induced electric fields in MRI. However, the following procedure could be adopted to include them. Instead of conditions (4a) and (4b), the solenoidality of the total (conduction and dielectric) current density is exploited:

$$\nabla \cdot \left\{ \sigma \left( \nabla \varphi_M \right) + \varepsilon \left[ \frac{\partial \left( \nabla \varphi_M \right)}{\partial t} \right]_M \right\} = -\nabla \cdot \left[ \sigma \left( \frac{\partial \boldsymbol{A}}{\partial t} \right)_M + \varepsilon \left( \frac{\partial^2 \boldsymbol{A}}{\partial t^2} \right)_M \right] \quad (6a)$$

$$\nabla \cdot \left\{ \sigma \left( \nabla \varphi_R \right) + \varepsilon \left[ \frac{\partial \left( \nabla \varphi_R \right)}{\partial t} \right]_M \right\} = \nabla \cdot \left\{ \sigma \left( \boldsymbol{v} \times \boldsymbol{B} \right) + \varepsilon \left[ \frac{\partial \left( \boldsymbol{v} \times \boldsymbol{B} \right)}{\partial t} \right]_M \right\} \quad (6b)$$

where, assuming a negligible effect of dispersion in frequency, $\varepsilon$ has been taken out of the time derivatives. Note that all time derivatives must be evaluated in M, even when applied to quantities defined in R [12]. From (6a) and (6b), relations analogous to (5a) and (5b), but including the dielectric terms, can be derived. The solution of such problems can be obtained again according to the FE method, but inserted within a classical time-stepping (e.g. Crank-Nicolson) scheme to handle the presence of the time derivative in the left-hand side.

### D. Procedure for exposure assessment

The human body is modeled through the "Duke" model belonging to the Virtual Family dataset [13]. It represents the body of an adult male, 1.77 m high, and is composed of 77 different tissues, whose electrical conductivity has been extrapolated from the data available in [14], by adopting a 4$^{th}$-order Cole-Cole dispersion model and a reference frequency of 1 Hz. The model has been segmented into cubic voxels with a resolution of 4 mm. Since the attention will be focused on the head, the model has been truncated just below the shoulders, having preliminarily verified that this operation does not alter the results within the head significantly. The total number of effective voxels involved in the simulations is about 265000, but only those above the chin (about 71000) will be considered in the final evaluation. For the computation of the exposure index recommended by ICNIRP [3], the following procedure has been adopted. First, the time signal of each Cartesian component of $E_M$ is determined by solving (5a) or (5b) for all voxels. Then, the three signals associated to a given voxel are processed according to the "weighted peak approach" [15], based on a Discrete Fourier Transform (DFT), to get the weighted signal:

$$W(t) = \sqrt{\sum_{k=1}^{3} \left\{ \left[ \sum_i^N \frac{A_i}{L_i} \cos\left( 2\pi f_i t + \theta_i + \delta_i \right) \right]^2 \right\}_k} \quad (7)$$

where index $k$ indicates the three Cartesian components of the induced signal, index $i$ indicates the order of the harmonic ($f$, $A$ and $\theta$ are its frequency, amplitude and phase, respectively), $L$ is the basic restriction and $\delta$ is the characteristic angle of the weighting function. The values of $L$ and $\delta$ are given, in frequency domain, in Table I. They have been taken from [3] and extended above 1 Hz according to [16]. In order to get the worst case evaluation, the adopted limits refer to "uncontrolled conditions" [3] and to the central nervous system of the head [16]. The ICNIRP guidelines define the exposure index as the peak of $W(t)$, which should be lower than 1 to get compliance.

## III. RESULTS AND DISCUSSION

An example of exposure assessment is presented here considering a realistic tubular MRI scanner, whose features have been provided by a manufacturer under a non-disclosure agreement. The scanner operates at 3 T and its axis is located 1 m above the ground. Two motion trajectories are considered. In the first one, the human model faces the bore of the scanner and then performs a 180° rotation around its own axis, in 1 s. The rotation includes a phase with constant acceleration (0.18 s), a phase with uniform angular speed of 3.83 rad/s (0.64 s) and a final phase with constant deceleration, which reduces the speed to zero (0.18 s). At the starting position, the face of the model is at an axial distance of 25 cm from the most external coil of the scanner. During the rotation, the minimum axial distance, got by the right shoulder, is 0.12 cm (this minimum distance is required to take into account the external size of the scanner, which contains a cryostat around the coils). The second trajectory is a 1 m translation along the axis of the scanner, starting from the final position of the previous movement (it simulates the man going away from the scanner). The translation includes a phase of constant acceleration (0.18 s), a uniform motion at 1.22 m/s (0.64 s) and a final constant deceleration (0.18 s). Both trajectories have been discretized into regular time steps, 0.02 s long. The distributions of $\boldsymbol{B}$ and $\boldsymbol{A}$ have been preliminarily defined on a grid of points with a spatial step of 2.5 cm (along the three directions). Apart from this preliminary evaluation, each simulation required about 5 hours (on an AMD Opteron 6276, 2.3 GHz, 16 cores server, in Windows HPC environment, using NVIDIA Tesla 2075 GPU cards).

The results of the assessment are summarized in Table II, which compares the maximum exposure indexes found for the

TABLE II
MAXIMUM EXPOSURE INDEX

| Trajectory | Version (5a) | Version (5b) |
|---|---|---|
| Rotation | 0.40 | 0.34 |
| Translation | 0.55 | 0.54 |
| Joined | 0.43 | 0.41 |

two trajectories following (5a) or (5b). The same table also shows the maximum exposure indexes obtained by joining the two trajectories as a sequence, without any break. Despite the quite high values of speed adopted, compliance with the ICNIRP Guidelines has been found in the present examples. However, this cannot exclude the possibility of violation in case of a more extended survey. Concerning this, it is clear from (5a) and (5b) that the results scale linearly with $\boldsymbol{B}$ (if its distribution keeps the same). The magnitude of the induced signals scales linearly also with $\boldsymbol{v}(t)$, but this does not reflect directly on the exposure index. Indeed, for a given displacement, an increase of the speed implies a reduction of the time needed to cover the distance and therefore a change of the harmonic spectrum (note that the basic restriction becomes more severe as frequency increases). The results given by the two computational approaches are in quite good agreement, but (5a) provided exposure indexes a bit higher than (5b). From spot checks in correspondence of some voxels (not reported for brevity), it seems that the induced signals are very "smooth" in case of (5b), while they are slightly more irregular (involving higher harmonic components) when computed through (5a). This suggest that (5a) is more sensitive from a numerical viewpoint. Moreover, (5b) has the advantage of allowing as an input a map of the magnetic flux density obtained experimentally, whereas the same cannot be done for the vector potential required by (5a). The maximum exposure index computed by joining the two trajectories is lower than the one obtained for the translation. This effect is a "physiological" outcome of the use of a DFT, which requires the identification of a specific observation time-window. Considering the effect of such arbitrariness, more specific indication about the implementation of the assessment procedure would be desirable.

If the simulations are repeated by adopting equations (6a) and (6b), the results given in Table II change less than 2%.

## APPENDIX – EQUIVALENCE BETWEEN DRIVING TERMS

Under the Galilean Magnetic Limit, the scalar potential transforms as $\varphi_M = \varphi_R - \boldsymbol{v}\cdot\boldsymbol{A}$ [9]. Strictly speaking, such transformation is valid for inertial frames, but, according to our working hypotheses, it is applied here, anyway. Thus, comparing (2b) and (3), we get

$$\boldsymbol{v}\times\boldsymbol{B} = \left[\nabla\left(\boldsymbol{v}\cdot\boldsymbol{A}\right)\right] - \left[\frac{\partial \boldsymbol{A}}{\partial t}\right]_M$$

$$= \left[\left(\boldsymbol{v}\cdot\nabla\right)\boldsymbol{A} + \left(\boldsymbol{A}\cdot\nabla\right)\boldsymbol{v} + \underbrace{\boldsymbol{v}\times\nabla\times\boldsymbol{A}}_{\boldsymbol{v}\times\boldsymbol{B}} + \boldsymbol{A}\times\nabla\times\boldsymbol{v}\right] - \left[\frac{\partial \boldsymbol{A}}{\partial t}\right]_M$$

In order to be verified, this equivalence requires:

$$\left(\boldsymbol{v}\cdot\nabla\right)\boldsymbol{A} + \left(\boldsymbol{A}\cdot\nabla\right)\boldsymbol{v} + \boldsymbol{A}\times\left(\nabla\times\boldsymbol{v}\right) - \left[\frac{\partial \boldsymbol{A}}{\partial t}\right]_M = 0$$

Introducing the transformation for the partial time derivative and exploiting some vector identities [12], the previous relation is verified, QED:

$$\left(\boldsymbol{v}\cdot\nabla\right)\boldsymbol{A} + \left(\boldsymbol{A}\cdot\nabla\right)\boldsymbol{v} + \boldsymbol{A}\times\left(\nabla\times\boldsymbol{v}\right) + \underbrace{-\left[\frac{\partial \boldsymbol{A}}{\partial t}\right]_R}_{0} + \boldsymbol{\omega}\times\boldsymbol{A} - \left(\boldsymbol{v}\cdot\nabla\right)\boldsymbol{A}$$

$$= \left(\boldsymbol{A}\cdot\nabla\right)\boldsymbol{v} + \boldsymbol{A}\times\left(\nabla\times\boldsymbol{v}\right) + \boldsymbol{\omega}\times\boldsymbol{A}$$

$$= \boldsymbol{\omega}\times\boldsymbol{A} + \boldsymbol{A}\times 2\boldsymbol{\omega} + \boldsymbol{\omega}\times\boldsymbol{A} = 0$$

## ACKNOWLEDGMENT

This work was supported by the European Metrology Research Programme (EMRP)-HLT06 Joint Research Project (JRP) "Metrology for next-generation safety standards and equipment in MRI" (2012–2015). The authors acknowledge Dr. D. Giordano and Dr. G. Bordonaro for their contributions.

## REFERENCES

[1] A. Amjad A., R. Kamondetdacha, A. V. Kildishev, and J. A. Nyenhuis, "Power deposition inside a phantom for testing of MRI heating," *IEEE Trans. Magn.*, vol. 41, pp. 4185-4187, Oct. 2005.

[2] H. Sanchez Lopez et al., "Modal Analysis of Currents Induced by Magnetic Resonance Imaging Gradient Coils," *IEEE Trans. Magn.*, vol. 50, pp. 7023404, Feb. 2014.

[3] International Commission on Non-Ionizing Radiation Protection, "Guidelines for Limiting Exposure to Electric Fields Induced by Movement of the Human Body in a Static Magnetic Field and by Time-Varying Magnetic Fields below 1 Hz," *Health Phys.*, vol. 106, pp. 418-425, Mar. 2014.

[4] L. Zilberti, O. Bottauscio, and M. Chiampi, "Motion-Induced Fields in Magnetic Resonance Imaging: Are the Dielectric Currents Really Negligible?," *IEEE Magnetics Letters*, vol. 6, pp. 1500104, May 2015.

[5] A. Trakic, L. Liu, H. Sanchez Lopez, L. Zilberti, F. Liu, and S. Crozier "Numerical safety study of currents induced in the patient during rotations in the static field produced by a hybrid MRI-LINAC system," *IEEE Trans. Biom. Eng.*, vol. 61, pp. 784-793, Mar. 2014.

[6] I. Laakso, S. Kannala, and K. Jokela K., "Computational dosimetry of induced electric fields during realistic movements in the vicinity of a 3 T MRI scanner," *Phys. Med. Biol.*, vol. 58, pp. 2625-2640, Apr. 2013.

[7] M. Chiampi, and L. Zilberti, "Induction of Electric Field in Human Bodies Moving Near MRI: an Efficient BEM Computational Procedure," *IEEE Trans. Biom. Eng.*, vol. 58, pp. 2787-2793, Oct. 2011.

[8] C. Cobos Sanchez, et al., "Forward electric field calculation using BEM for time-varying magnetic field gradients and motion in strong static fields," *Eng. Anal. Bound. Elem.*, vol. 33, pp. 1074-1088, Aug. 2009.

[9] F. Rapetti, and G. Rousseaux, "Implications of Galilean electromagnetism in numerical modeling," *Appl. Comput. Electrom.*, vol. 26, pp. 784-791, Sep. 2011.

[10] J. G. Van Bladel, *Electromagnetic Fields*, Piscataway, NJ, USA, IEEE Press, 2007.

[11] S. Kurz, B. Flemisch, and B. Wohlmuth, "Maxwell's equations in accelerated reference frames and their application in computational electromagnetism," Proc. Progr. Electromagn. Res. Symp., Pisa, Italy, pp. 53–56, available: http://www.piers.org/piers2k4Pisa/.

[12] K. T. McDonald, "Electrodynamics of rotating systems," Available: http://www.hep.princeton.edu/~mcdonald/examples/rotatingEM.pdf.

[13] A. Christ, et al., "The Virtual Family - development of surface-based anatomical models of two adults and two children for dosimetric simulations," *Phys. Med. Biol.*, vol. 55, pp. N23-N38, Jan. 2010.

[14] P. A. Hasgall, E. Neufeld, M. C. Gosselin, A. Klingenböck, and N. Kuster. (Jan. 2015). IT'IS Database for Thermal and Electromagnetic Parameters of Biological Tissues, Version 2.6. [Online]. Available: http://www.itis.ethz.ch/database.

[15] International Commission on Non-Ionizing Radiation Protection, “Guidance on determining compliance of exposure to pulsed and complex non-sinusoidal waveforms below 100 kHz with ICNIRP guidelines,” *Health Phys.*, vol. 84, pp. 83–387, 2003.
[16] International Commission on Non-Ionizing Radiation Protection, “Guidelines for limiting exposure to time-varying electric and magnetic fields (1 Hz to 100 kHz),” *Health Phys*. vol. 99, pp. 818-836, 2010.